Electronic Supplementary Material (ESI) for Dalton Transactions.

Electronic Supporting Information Materials

Cell nucleus localization and high anticancer activity of quinoline-benzopyran rhodium(III) metal complexes as therapeutic and fluorescence imaging agents

Zhen-Feng Wang [a,b], Xiao-Ling Nai [c], Yue Xu [c], Feng-Hua Pan [c], Fu-Shun Tang [a,*]

Qi-Pin Qin [c], Lin Yang [c], Shu-Hua Zhang [a,b,*]

Table S1. Crystal data and structure refinement details for **RhN1**.

Empirical formula	$C_{16}H_{15}Cl_4N_2O_2RhS$
Formula weight	544.07
Crystal system	triclinic
Space group	*P*-1
a/Å	8.066(1)
b/Å	8.563(1)
c/Å	14.400(1)
α/°	78.253(3)
β/°	84.796(3)
γ/°	86.950(3)
V/Å^3	969.08(14)
Z	2
D_c (g cm^{-3})	1.865
μ/mm^{-1}	1.554
F(000)	540
Crystal size/mm^3	0.37 × 0.28 × 0.14
Radiation	MoKα (λ = 0.71073 Å)
2Θ range for data collection/°	6.048 to 55.194
Index ranges	$-10 \leq h \leq 10$, $-11 \leq k \leq 11$, $-18 \leq l \leq 18$
Reflections collected	20866
Independent reflections	4486 [R_{int} = 0.0484, R_{sigma} = 0.0506]
Data/restraints/parameters	4486/0/240
Goodness-of-fit on F^2	1.070
Final R indexes [$I \geq 2\sigma(I)$]	R_1 = 0.0349, wR_2 = 0.0752
Final R indexes [all data]	R_1 = 0.0625, wR_2 = 0.0821
Largest diff. peak/hole / e Å^{-3}	0.453/-0.612

^{a} $R_1 = \Sigma ||F_o| - |F_c||/\Sigma|F_o|$; ^{b} $wR_2 = [\Sigma w(F_o^2 - F_c^2)^2/\Sigma w(F_o^2)^2]^{½}$.

Table S2. Selected bond lengths (Å) for **RhN1**.

Atom	Atom	Length/Å	Atom	Atom	Length/Å
Rh1	S1	2.2655(8)	C3	C4	1.376(5)
Rh1	N1	2.077(2)	C3	C2	1.364(5)
Rh1	N2	2.019(3)	C5	C6	1.485(4)
Rh1	Cl2	2.3462(9)	C5	C4	1.392(4)
Rh1	Cl3	2.3346(9)	C6	C7	1.458(4)
Rh1	Cl1	2.3342(9)	C6	C8	1.347(4)
S1	O2	1.469(2)	C1	C2	1.369(4)
S1	C15	1.775(3)	C10	C9	1.377(4)
S1	C16	1.767(3)	C10	C11	1.381(5)
Cl4	C13	1.731(4)	C8	C9	1.432(4)
N1	C5	1.357(4)	C9	C14	1.394(5)
N1	C1	1.337(4)	C12	C13	1.382(5)
N2	C7	1.265(4)	C12	C11	1.379(5)
O1	C7	1.349(4)	C14	C13	1.375(5)
O1	C10	1.380(4)			

Table S3. Selected bond angles (°) for **RhN1**.

Atom	Atom	Atom	Angle/°	Atom	Atom	Atom	Angle/°
S1	Rh1	Cl2	92.75(3)	C2	C3	C4	118.4(3)
S1	Rh1	Cl3	90.25(3)	N1	C5	C6	121.5(3)
S1	Rh1	Cl1	88.09(3)	N1	C5	C4	119.3(3)
N1	Rh1	S1	177.30(7)	C4	C5	C6	119.2(3)
N1	Rh1	Cl2	88.39(7)	C7	C6	C5	122.3(3)
N1	Rh1	Cl3	88.55(7)	C8	C6	C5	120.6(3)
N1	Rh1	Cl1	94.35(7)	C8	C6	C7	117.1(3)
N2	Rh1	S1	89.39(8)	N2	C7	O1	116.0(3)
N2	Rh1	N1	88.20(10)	N2	C7	C6	124.7(3)
N2	Rh1	Cl2	87.80(9)	O1	C7	C6	119.3(3)
N2	Rh1	Cl3	90.70(9)	C3	C4	C5	120.8(3)
N2	Rh1	Cl1	176.80(9)	N1	C1	C2	122.6(3)
Cl3	Rh1	Cl2	176.64(3)	O1	C10	C11	117.2(3)
Cl1	Rh1	Cl2	90.35(3)	C9	C10	O1	120.1(3)
Cl1	Rh1	Cl3	91.28(4)	C9	C10	C11	122.7(3)

O2	S1	Rh1	112.82(10)	C6	C8	C9	122.5(3)
O2	S1	C15	108.02(16)	C3	C2	C1	119.5(3)
O2	S1	C16	109.35(16)	C10	C9	C8	118.0(3)
C15	S1	Rh1	113.11(13)	C10	C9	C14	118.7(3)
C16	S1	Rh1	112.25(13)	C14	C9	C8	123.3(3)
C16	S1	C15	100.54(18)	C11	C12	C13	120.1(3)
C5	N1	Rh1	123.1(2)	C13	C14	C9	118.9(3)
C1	N1	Rh1	117.6(2)	C12	C13	Cl4	119.5(3)
C1	N1	C5	119.3(3)	C14	C13	Cl4	118.9(3)
C7	N2	Rh1	122.4(2)	C14	C13	C12	121.6(3)
C7	O1	C10	121.5(2)	C12	C11	C10	118.0(3)

Table S4. Crystal data and structure refinement details for **RhN2**.

Empirical formula	$C_{18}H_{17}BrCl_3N_2O_4Rh$
Formula weight	614.50
Crystal system	triclinic
Space group	*P*-1
a/Å	7.932(1)
b/Å	10.497(1)
c/Å	14.048(1)
α/°	103.36(1)
β/°	103.59(1)
γ/°	100.60(1)
V/Å^3	1070.6(2)
Z	2
D_c(g/cm^3)	1.906
μ/mm^{-1}	3.066
F(000)	604
Crystal size/mm^3	0.22 × 0.18 × 0.15
Radiation	MoKα (λ = 0.71073 Å)
Θ range for data collection/°	3.266 to 25.10
Index ranges	$-9 \le h \le 9$, $-10 \le k \le 12$, $-16 \le l \le 16$
Reflections collected	6502
Independent reflections	3810 [R_{int} = 0.0285, R_{sigma} = 0.0618]
Data/restraints/parameters	3810/14/263
Goodness-of-fit on F^2	0.993
Final R indexes [$I \geq 2\sigma (I)$]	R_1 = 0.0508, wR_2 = 0.0924
Final R indexes [all data]	R_1 = 0.0750, wR_2 = 0.1054
Largest diff. peak/hole / e Å^{-3}	1.037/-0.700

[a] $R_1 = \Sigma ||F_o| - |F_c||/\Sigma|F_o|$; [b] $wR_2 = [\Sigma w(F_o^2 - F_c^2)^2/\Sigma w(F_o^2)^2]^{1/2}$.

Table S5. Selected bond lengths (Å) for **RhN2**.

Atom	Atom	Length/Å	Atom	Atom	Length/Å
Rh1	Cl1	2.334(2)	C1	C6	1.388(9)
Rh1	Cl2	2.299(2)	C2	C3	1.378(10)
Rh1	Cl3	2.326(2)	C3	C4	1.389(11)
Rh1	O1	2.195(4)	C4	C5	1.362(11)
Rh1	N2	1.999(5)	C5	C6	1.399(10)
Rh1	O4	2.055(5)	C7	C8	1.458(9)
Br1	C15	1.897(7)	C8	C9	1.470(9)
O1	C17	1.297(8)	C8	C10	1.365(8)
O3	C9	1.348(8)	C10	C11	1.415(9)
O3	C12	1.391(7)	C11	C12	1.386(9)
N1	C6	1.372(9)	C11	C16	1.408(9)
N1	C7	1.344(8)	C12	C13	1.362(10)
N2	C1	1.410(8)	C13	C14	1.372(9)
N2	C7	1.336(8)	C14	C15	1.385(10)
O4	C9	1.251(7)	C15	C16	1.363(10)
C1	C2	1.391(10)	O2	C18	1.249(8)

Table S6. Selected bond angles (°) for **RhN2**.

Atom	Atom	Atom	Angle/°	Atom	Atom	Atom	Angle/°
Cl2	Rh1	Cl1	90.69(8)	C5	C4	C3	121.4(8)
Cl2	Rh1	Cl3	91.46(8)	C4	C5	C6	116.7(8)
Cl3	Rh1	Cl1	177.82(8)	N1	C6	C1	106.6(6)
O1	Rh1	Cl1	90.43(12)	N1	C6	C5	131.5(7)
O1	Rh1	Cl2	88.40(11)	C1	C6	C5	121.9(7)
O1	Rh1	Cl3	89.31(12)	N1	C7	C8	122.2(6)
N2	Rh1	Cl1	90.06(15)	N2	C7	N1	111.6(6)
N2	Rh1	Cl2	95.64(16)	N2	C7	C8	126.2(6)
N2	Rh1	Cl3	90.05(15)	C7	C8	C9	120.0(5)
N2	Rh1	O1	175.93(19)	C10	C8	C7	121.8(6)
N2	Rh1	O4	88.5(2)	C10	C8	C9	118.4(6)
O4	Rh1	Cl1	87.01(14)	O3	C9	C8	118.2(6)
O4	Rh1	Cl2	175.23(15)	O4	C9	O3	116.2(6)
O4	Rh1	Cl3	90.81(14)	O4	C9	C8	125.6(6)

O4	Rh1	O1	87.44(16)	C8	C10	C11	122.0(6)
C17	O1	Rh1	121.1(5)	C10	C11	C16	123.4(7)
C9	O3	C12	123.0(5)	C12	C11	C10	118.6(6)
C7	N1	C6	108.1(6)	C12	C11	C16	118.0(7)
C1	N2	Rh1	130.6(4)	O3	C12	C11	119.6(6)
C7	N2	Rh1	123.4(4)	C13	C12	O3	117.5(6)
C7	N2	C1	105.6(5)	C13	C12	C11	122.7(6)
C9	O4	Rh1	124.1(4)	C12	C13	C14	118.9(7)
C2	C1	N2	131.2(7)	C13	C14	C15	119.7(7)
C2	C1	C6	120.7(7)	C14	C15	Br1	119.4(6)
C6	C1	N2	108.0(6)	C16	C15	Br1	118.7(6)
C1	C2	C3	116.4(7)	C16	C15	C14	121.9(7)
C4	C3	C2	122.6(8)	C15	C16	C11	118.8(7)

Table S7. Crystal data and structure refinement details for **RhS**.

Empirical formula	$C_{22}H_{25}Cl_3NO_4RhS$
Formula weight	608.75
Crystal system	triclinic
Space group	*P*-1
a/Å	11.859(1)
b/Å	13.461(1)
c/Å	15.836(1)
α/°	80.727(6)
β/°	87.740(5)
γ/°	80.679(6)
V/Å^3	2461.8(3)
Z	4
D_c(g/cm^3)	1.643
μ/mm^{-1}	1.133
F(000)	1232
Crystal size/mm^3	0.36 × 0.25 × 0.18
Radiation	MoKα (λ = 0.71073)
Θ range for data collection/°	3.367 to 25.10
Index ranges	$-14 \leq h \leq 13$, $-15 \leq k \leq 16$, $-18 \leq l \leq 18$
Reflections collected	16384
Independent reflections	8734 [R_{int} = 0.0370, R_{sigma} = 0.0660]
Data/restraints/parameters	8734/30/588
Goodness-of-fit on F^2	1.005
Final R indexes [$I \geq 2\sigma (I)$]	R_1 = 0.0502, wR_2 = 0.1146
Final R indexes [all data]	R_1 = 0.0805, wR_2 = 0.1396

Largest diff. peak/hole / e Å^{-3}	0.911/-0.998

^{a} $R_1 = \Sigma ||F_o| - |F_c||/\Sigma|F_o|$; ^{b} $wR_2 = [\Sigma w(F_o^2 - F_c^2)^2/\Sigma w(F_o^2)^2]^{½}$.

Table S8. Selected bond lengths (Å) for **RhS**.

Atom	Atom	Length/Å	Atom	Atom	Length/Å
Rh1	Cl4	2.319(2)	Rh2	Cl2	2.298(2)
Rh1	Cl5	2.301(2)	Rh2	Cl3	2.313(2)
Rh1	Cl6	2.345(2)	Rh2	O4	2.074(4)
Rh1	O2	2.054(4)	Rh2	O8	2.071(4)
Rh1	N1	2.027(5)	Rh2	N2	2.022(4)
Rh1	O7	2.055(4)	S2	C27	1.712(6)
S1	C6	1.721(6)	S2	C28	1.718(5)
S1	C7	1.730(6)	O3	C30	1.233(6)
O1	C9	1.336(6	O3	C37	1.386(6)
O1	C16	1.392(6)	O4	C42	1.434(7)
O2	C21	1.414(7)	O8	C30	1.229(6)
N1	C9	1.228(6)	N2	C22	1.402(7)
O7	C1	1.407(7)	N2	C28	1.333(7)
O7	C7	1.320(7)	C22	C23	1.398(8)
C1	C2	1.394(8)	C22	C27	1.391(8)
C1	C6	1.387(8)	C23	C24	1.376(9)
C2	C3	1.375(9)	C24	C25	1.376(10)
C3	C4	1.417(10)	C25	C26	1.390(9)
C4	C5	1.362(10)	C26	C27	1.393(8)
C5	C6	1.416(8)	C28	C29	1.457(8)
C7	C8	1.457(7)	C29	C30	1.438(8)
C8	C9	1.444(8)	C29	C31	1.349(7)
C8	C10	1.351(8)	C31	C32	1.428(8)
C10	C11	1.432(8)	C32	C33	1.415(7)
C11	C12	1.422(8)	C32	C37	1.382(8)
C11	C16	1.386(8)	C33	C34	1.358(9)
C12	C13	1.358(8)	C34	C35	1.385(9)
C13	C14	1.380(9)	C35	C36	1.402(8)
C14	C15	1.386(8)	C36	C37	1.389(8)
C15	C16	1.394(8)	C36	C38	1.520(9)
C15	C17	1.525(8)	C38	C39	1.518(11)
C17	C18	1.522(9)	C38	C40	1.529(10)
C17	C19	1.540(10)	C38	C41	1.553(10)
C17	C20	1.539(9)	O5	C43	1.297(12)

Rh2	Cl1	2.352(2)	O6	C44	1.315(9)

Table S9. Selected bond angles (°) for **RhS**.

Atom	Atom	Atom	Angle/°	Atom	Atom	Atom	Angle/°
Cl4	Rh1	Cl6	175.36(6)	Cl2	Rh2	Cl1	88.58(6)
Cl5	Rh1	Cl4	94.81(6)	Cl2	Rh2	Cl3	93.60(6)
Cl5	Rh1	Cl6	88.95(6)	Cl3	Rh2	Cl1	175.99(7)
O2	Rh1	Cl4	88.88(15)	O4	Rh2	Cl1	87.05(13)
O2	Rh1	Cl5	85.99(1	O4	Rh2	Cl2	88.61(13)
O2	Rh1	Cl6	88.66(15)	O4	Rh2	Cl3	89.63(14)
N1	Rh1	Cl4	89.12(12)	O8	Rh2	Cl1	86.60(13)
N1	Rh1	Cl5	173.26(13	O8	Rh2	Cl2	173.74(13)
N1	Rh1	Cl6	86.89(12)	O8	Rh2	Cl3	90.98(13)
N1	Rh1	O2	88.61(17)	O8	Rh2	O4	87.16(17)
O7	Rh1	Cl4	90.10(13)	N2	Rh2	Cl1	91.94(13)
O7	Rh1	Cl5	97.10(14)	N2	Rh2	Cl2	96.02(14)
O7	Rh1	Cl6	92.14(13)	N2	Rh2	Cl3	91.18(13)
O7	Rh1	O2	176.82(19)	N2	Rh2	O4	175.24(18)
O7	Rh1	N1	88.36(17)	N2	Rh2	N3	88.14(18)
C6	S1	C7	89.9(3)	C27	S2	C28	90.2(3)
C9	O1	C16	123.3	C30	O3	C37	123.6(4)
C21	O2	Rh1	124.9(4)	C42	O4	Rh2	124.7(4)
C9	N1	Rh1	119.2(4)	C30	O8	Rh2	119.7(4)
C1	O7	Rh1	128.2(4)	C22	N2	Rh2	128.5(4)
C7	O7	Rh1	119.7(4)	C28	N2	Rh2	120.0(4)
C7	O7	C1	112.1(5)	C28	N2	C22	111.2(5)
C2	C1	O7	127.1(5)	C23	C22	N2	126.8(6)
C6	C1	O7	112.6(5)	C27	C22	N2	113.0(5)
C6	C1	C2	120.2(6)	C27	C22	C23	120.1(6)
C3	C2	C1	118.4(6)	C24	C23	C22	117.4(6)
C2	C3	C4	121.2(6)	C23	C24	C25	122.9(7)
C5	C4	C3	120.9(6)	C24	C25	C26	120.1(6)
C4	C5	C6	117.7(7)	C25	C26	C27	117.8(7)
C1	C6	S1	111.2(5)	C22	C27	S2	111.0(4
C1	C6	C5	121.5(6)	C22	C27	C26	121.4(6)
C5	C6	S1	127.3(5)	C26	C27	S2	127.5(5)
O7	C7	S1	114.1(4)	N2	C28	S2	114.4(4)
O7	C7	C8	127.1(5)	N2	C28	C29	126.5(5)
C8	C7	S1	118.8(4)	C29	C28	S2	119.1(4)

C9	C8	C7	119.2(5)	C30	C29	C28	120.4(5)
C10	C8	C7	122.2(5)	C31	C29	C28	120.2(5)
C10	C8	C9	118.3(5)	C31	C29	C30	119.1(5)
O1	C9	C8	119.6(4)	O3	C30	C29	118.8(4)
N1	C9	O1	114.3(5)	O8	C30	O3	126.4(5)
N1	C9	C8	126.2(5)	O8	C30	C29	126.5(5)
C8	C10	C11	121.3(5)	C29	C31	C32	121.0(5)
C12	C11	C10	121.7(5)	C33	C32	C31	121.9(5)
C16	C11	C10	119.4(5)	C37	C32	C31	119.0(5)
C16	C11	C12	118.9(5)	C37	C32	C33	119.1(5)
C13	C12	C11	117.7(6)	C34	C33	C32	118.6(6)
C12	C13	C14	120.9(6)	C33	C34	C35	120.8(6
C13	C14	C15	124.6(6)	C34	C35	C36	123.0(6)
C14	C15	C16	113.3(6)	C35	C36	C38	123.4(6)
C14	C15	C17	123.3(6)	C37	C36	C35	114.7(6)
C16	C15	C17	123.3(5)	C37	C36	C38	121.8(5)
O1	C16	C15	117.5(5	C32	C37	O3	118.4(5)
C11	C16	O1	118.1(5)	C32	C37	C36	123.8(5)
C11	C16	C15	124.5(5)	C36	C37	O3	117.8(5)
C15	C17	C19	108.7(6)	C36	C38	C39	110.2(6)
C15	C17	C20	111.1(5)	C36	C38	C40	111.1(6)
C18	C17	C15	111.4(5)	C36	C38	C41	110.5(6)
C18	C17	C19	110.3(6	C39	C38	C40	110.6(6)
C18	C17	C20	107.2(6)	C39	C38	C41	107.5(7)
C19	C17	C20	108.2(6)	C40	C38	C41	106.8(7)

Table S10. Crystal data and structure refinement details for **RhQ**.

Empirical formula	$C_{24}H_{26}Cl_3N_2O_2RhS$
Formula weight	615.79
Crystal system	triclinic
Space group	*P*-1
a/Å	8.3861(3)
b/Å	11.4423(4)
c/Å	13.9193(5)
α/°	78.158(1)
β/°	88.814(1)
γ/°	80.093(1)
V/Å^3	1287.58(8)
Z	2
D_c(g/cm^3)	1.588
μ/mm^{-1}	1.080

F(000)	624
Crystal size/mm^3	0.20 × 0.09 × 0.05
Radiation	MoKα (λ = 0.71073)
Θ range for data collection/°	2.99 to 25.10
Index ranges	$-10 \le h \le 10$, $-13 \le k \le 13$, $-16 \le l \le 16$
Reflections collected	23527
Independent reflections	4579 [R_{int} = 0.0338, R_{sigma} = 0.0290]
Data/restraints/parameters	4579/0/303
Goodness-of-fit on F^2	1.007
Final R indexes [$I \geq 2\sigma (I)$]	R_1 = 0.0242, wR_2 = 0.0549
Final R indexes [all data]	R_1 = 0.0345, wR_2 = 0.0584
Largest diff. peak/hole / e Å^{-3}	0.474/-0.551

[a] $R_1 = \Sigma ||F_o| - |F_c||/\Sigma|F_o|$; [b] $wR_2 = [\Sigma w(F_o^2 - F_c^2)^2/\Sigma w(F_o^2)^2]^{½}$.

Table S11. Selected bond lengths (Å) for **RhQ**.

Atom	Atom	Length/Å	Atom	Atom	Length/Å
Rh1	S1	2.2615(6)	C9	C10	1.486(3)
Rh1	Cl3	2.3313(6)	C9	C8	1.415(3)
Rh1	Cl1	2.3573(6)	C19	C17	1.534(3)
Rh1	Cl2	2.3596(6)	C19	C22	1.530(4)
Rh1	N2	2.0123(18)	C10	C12	1.349(3)
Rh1	N1	2.1357(18)	C13	C14	1.399(3)
S1	O2	1.4732(17)	C13	C12	1.429(3)
S1	C23	1.770(2)	C17	C16	1.391(4)
S1	C24	1.765(3)	C14	C15	1.372(4)
O1	C18	1.380(3)	C1	C6	1.417(3)
O1	C11	1.352(3)	C1	C2	1.404(3)
N2	C11	1.277(3)	C6	C5	1.416(3)
N1	C9	1.339(3)	C6	C7	1.390(4)
N1	C1	1.398(3)	C5	C4	1.343(4)
C18	C13	1.389(3)	C8	C7	1.349(3)
C18	C17	1.395(3)	C16	C15	1.382(4)
C11	C10	1.444(3)	C2	C3	1.369(3)
C21	C19	1.532(4)	C4	C3	1.394(4)
C20	C19	1.525(4)			

Table S12. Selected bond angles (°) for **RhQ**.

Atom	Atom	Atom	Angle/°	Atom	Atom	Atom	Angle/°
S1	Rh1	Cl3	92.27(2)	N1	C9	C8	121.3(2)
S1	Rh1	Cl1	86.96(2)	C8	C9	C10	115.3(2)
S1	Rh1	Cl2	86.98(2)	C21	C19	C17	111.0(2)
Cl3	Rh1	Cl1	86.89(2)	C20	C19	C21	109.6(2)
Cl3	Rh1	Cl2	175.69(2)	C20	C19	C17	109.8(2)
Cl1	Rh1	Cl2	97.30(2)	C20	C19	C22	107.1(2)
N2	Rh1	S1	87.63(5)	C22	C19	C21	107.6(2)
N2	Rh1	Cl3	89.15(6)	C22	C19	C17	111.7(2)
N2	Rh1	Cl1	173.16(6)	C11	C10	C9	122.0(2)
N2	Rh1	Cl2	86.57(6)	C12	C10	C11	116.3(2)
N2	Rh1	N1	86.99(7)	C12	C10	C9	121.6(2)
N1	Rh1	S1	174.59(5)	C18	C13	C14	118.6(2)
N1	Rh1	Cl3	88.08(5)	C18	C13	C12	118.9(2)
N1	Rh1	Cl1	98.44(5)	C14	C13	C12	122.5(2)
N1	Rh1	Cl2	92.27(5)	C18	C17	C19	123.8(2)
O2	S1	Rh1	111.88(7)	C16	C17	C18	114.0(2)
O2	S1	C23	108.10(12)	C16	C17	C19	122.2(2)
O2	S1	C24	108.19(12)	C15	C14	C13	118.9(3)
C23	S1	Rh1	113.52(9)	N1	C1	C6	120.5(2)
C24	S1	Rh1	113.40(9)	N1	C1	C2	121.4(2)
C24	S1	C23	101.06(14)	C2	C1	C6	118.0(2)
C11	O1	C18	122.64(17)	C5	C6	C1	119.2(2)
C11	N2	Rh1	121.41(15)	C7	C6	C1	118.6(2)
C9	N1	Rh1	119.46(14)	C7	C6	C5	122.0(2)
C9	N1	C1	118.56(19)	C4	C5	C6	121.2(3)
C1	N1	Rh1	121.84(15)	C7	C8	C9	120.5(2)
O1	C18	C13	118.1(2)	C10	C12	C13	122.8(2)
O1	C18	C17	117.4(2)	C8	C7	C6	119.9(2)
C13	C18	C17	124.5(2)	C15	C16	C17	123.6(3)
O1	C11	C10	120.14(19)	C3	C2	C1	120.4(2)
N2	C11	O1	115.45(19)	C14	C15	C16	120.5(3)
N2	C11	C10	124.4(2)	C5	C4	C3	119.6(2)
N1	C9	C10	123.25(19)	C2	C3	C4	121.3(3)

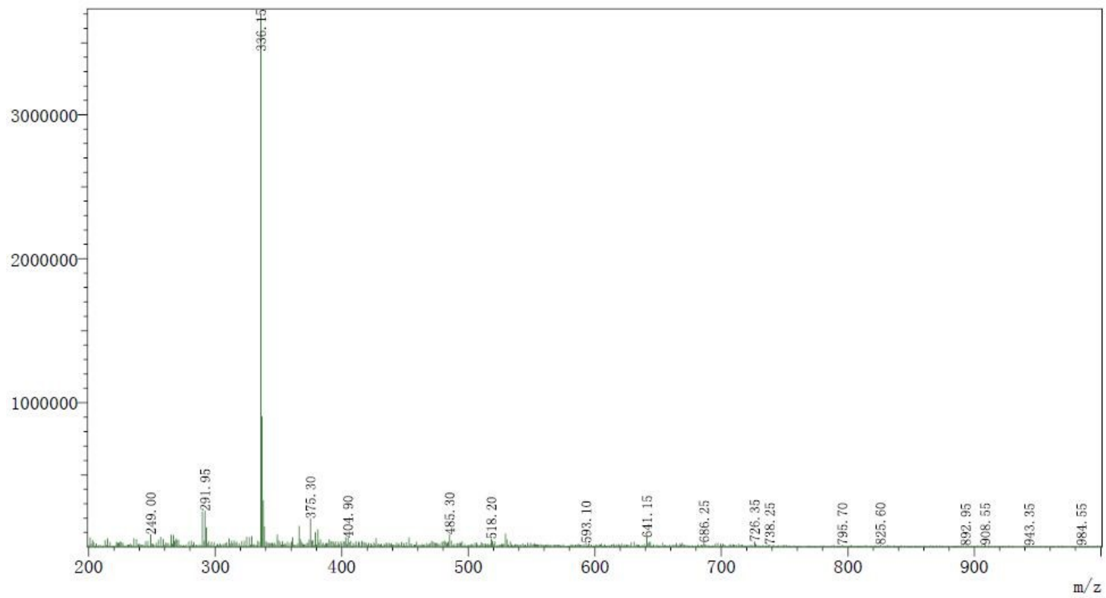

Figure S1. ESI-MS spectra of QB3a (2.0×10^{-5} M) in Tris-HCl buffer solution (containing 5% DMSO) for 0 h.

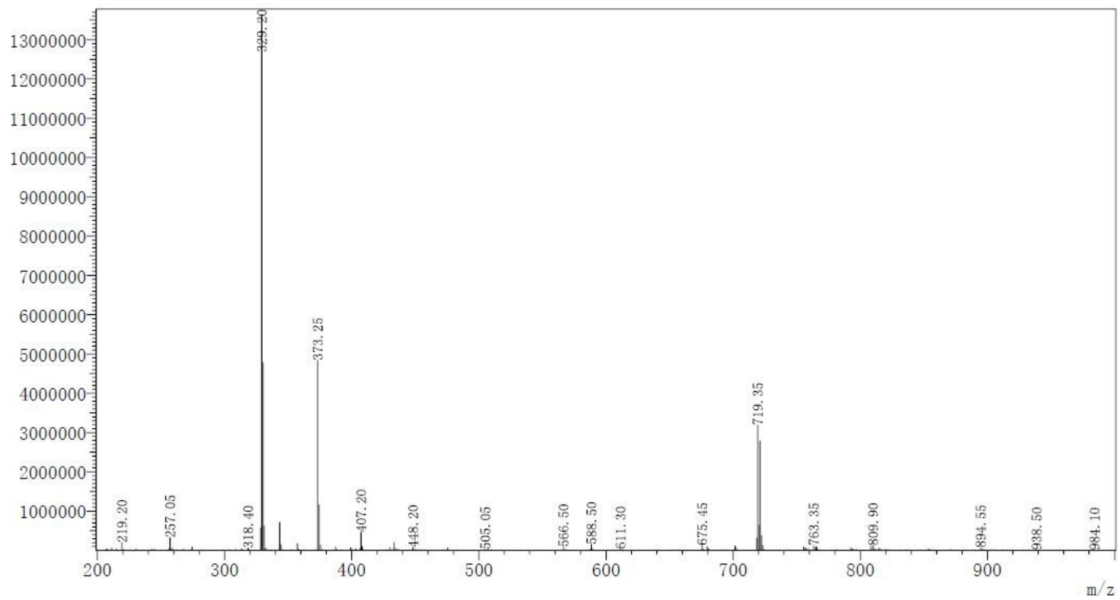

Figure S2. ESI-MS spectra of QB4 (2.0×10^{-5} M) in Tris-HCl buffer solution (containing 5% DMSO) for 0 h.

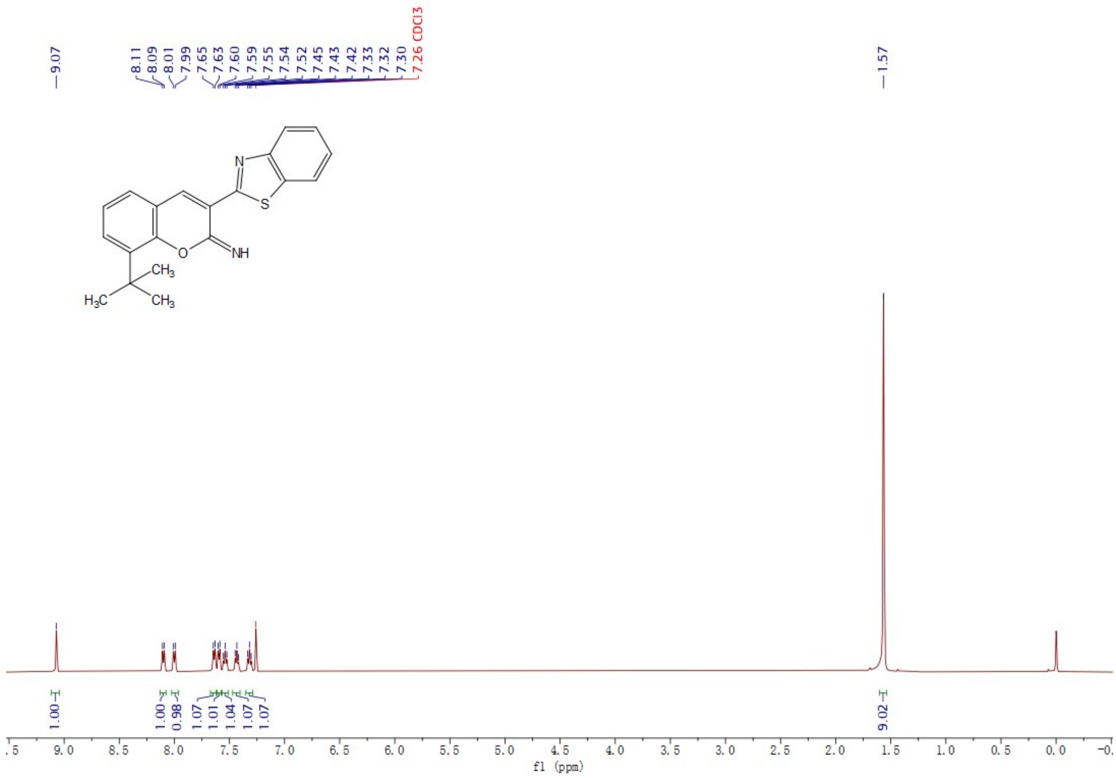

Figure S3. ^{1}H NMR (500MHz, DMSO-d_6) for QB3a.

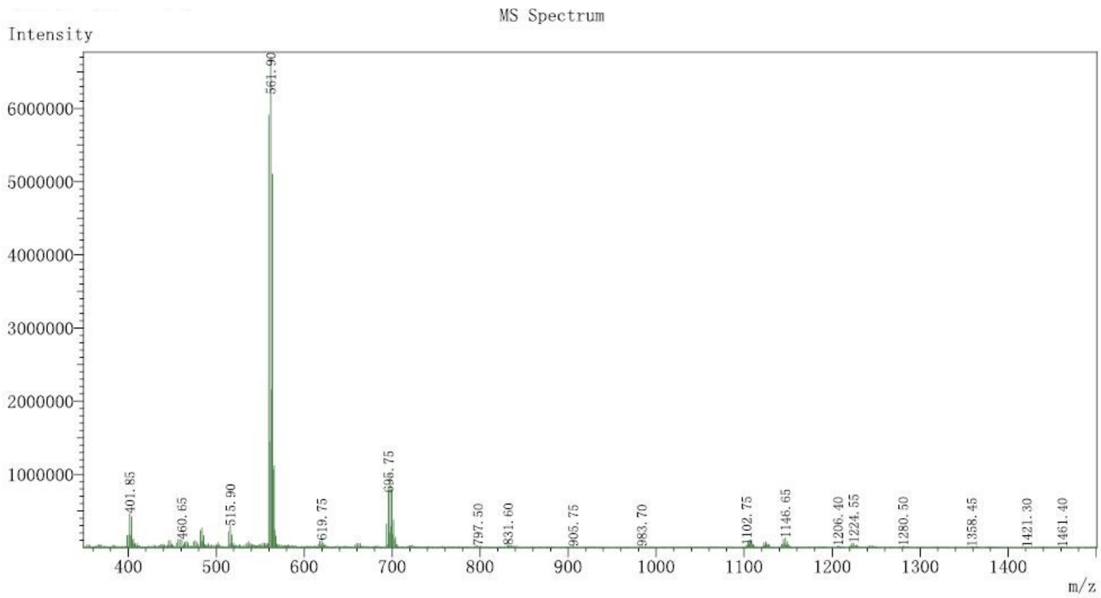

Figure S4. ESI-MS spectra of **RhN1** (2.0×10^{-5} M) in Tris-HCl buffer solution (containing 5% DMSO) for 0 h.

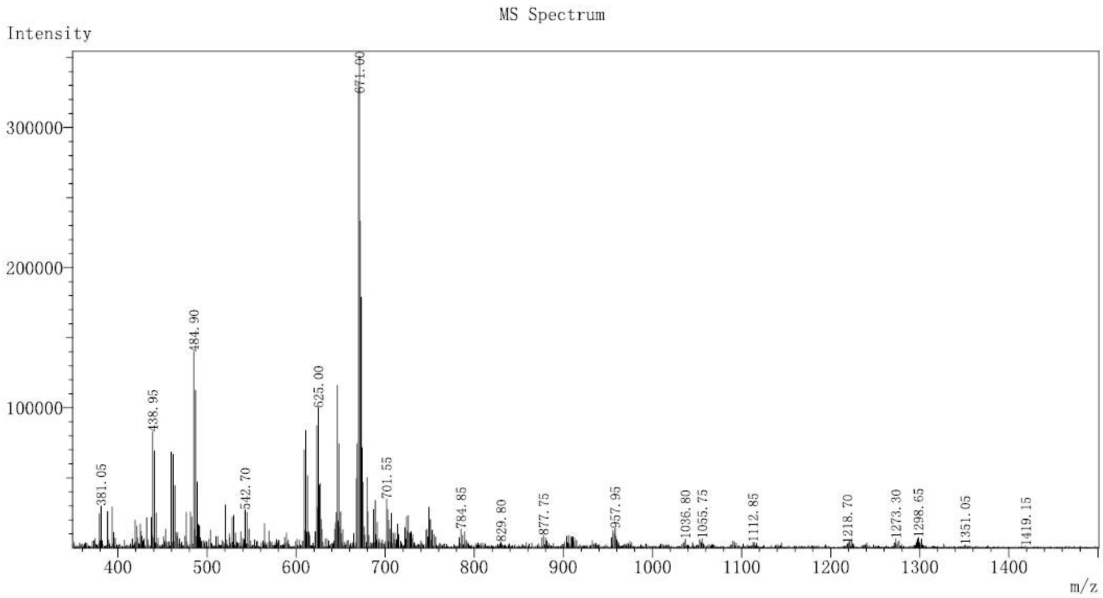

Figure S5. ESI-MS spectra of **RhN2** (2.0×10^{-5} M) in Tris-HCl buffer solution (containing 5% DMSO) for 0 h.

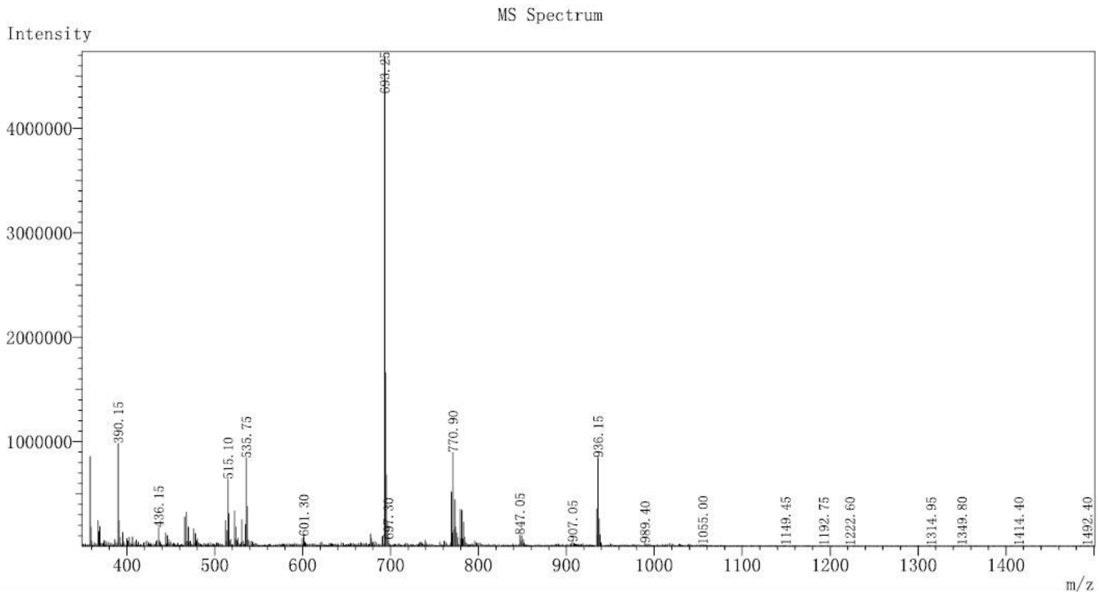

Figure S6. ESI-MS spectra of **RhS** (2.0×10^{-5} M) in Tris-HCl buffer solution (containing 5% DMSO) for 0 h.

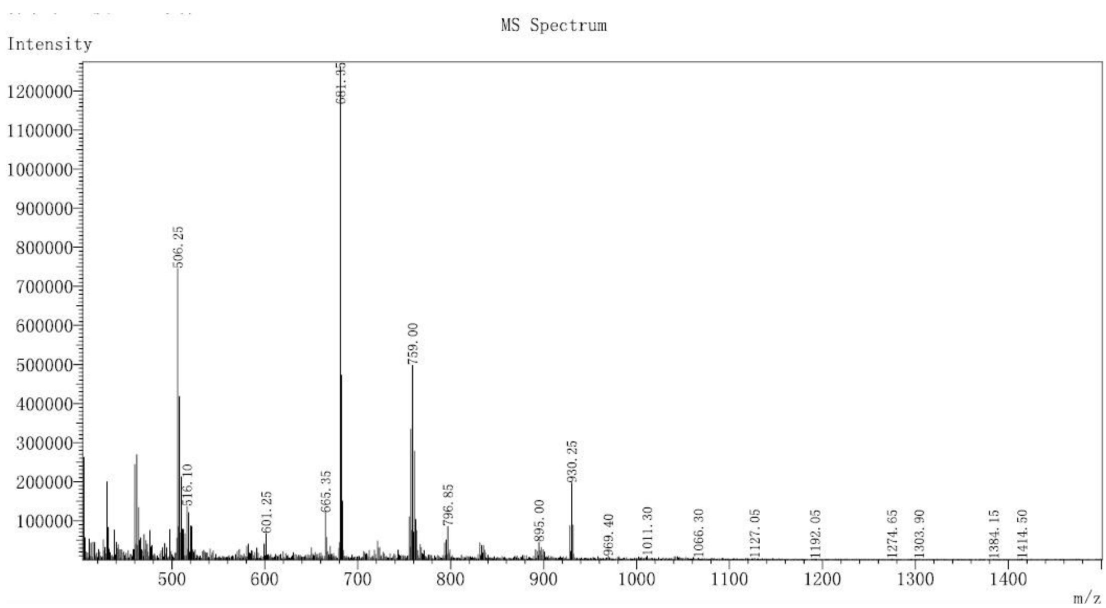

Figure S7. ESI-MS spectra of **RhQ** (2.0×10^{-5} M) in Tris-HCl buffer solution (containing 5% DMSO) for 0 h.

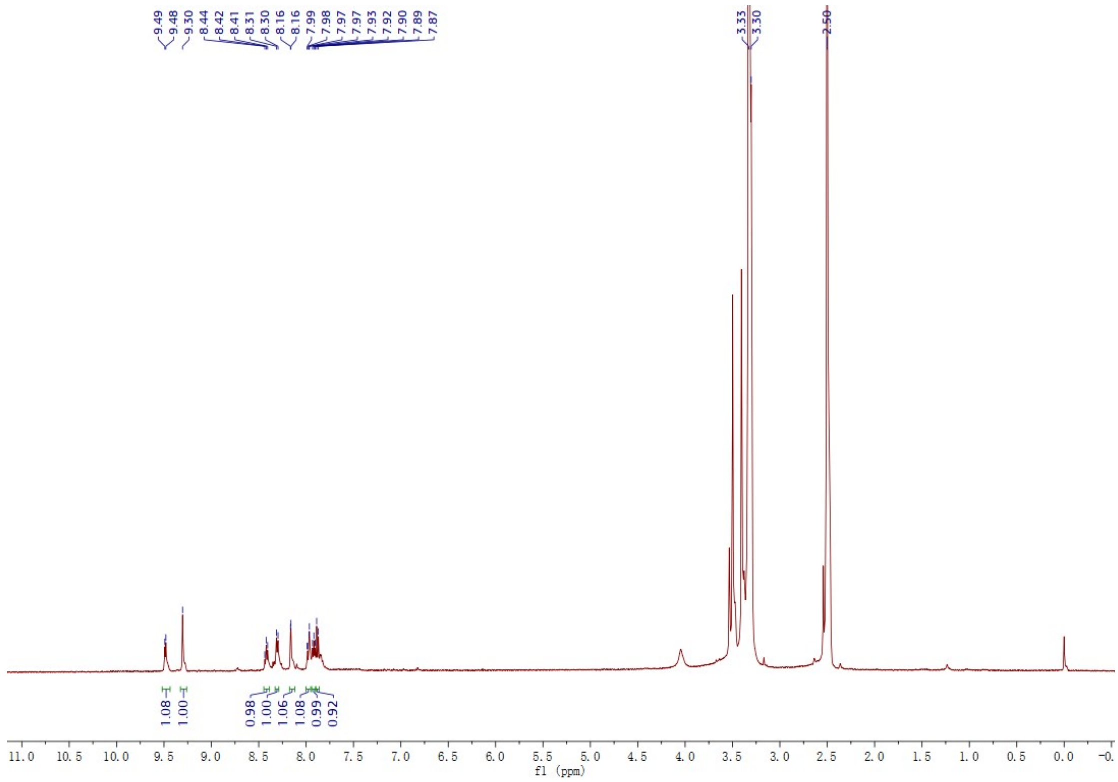

Figure S8. ^{1}H NMR (500MHz, DMSO-d_6) for **RhN1**.

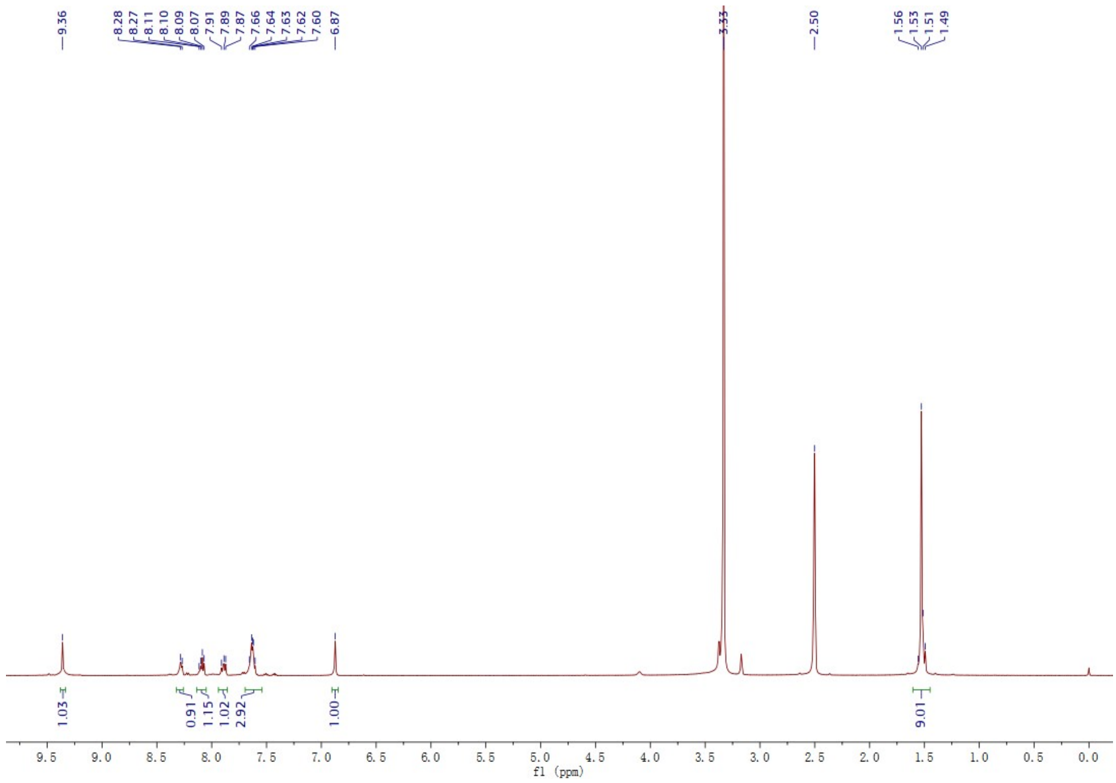

Figure S9. ^{1}H NMR (500MHz, DMSO-d_6) for **RhS**.

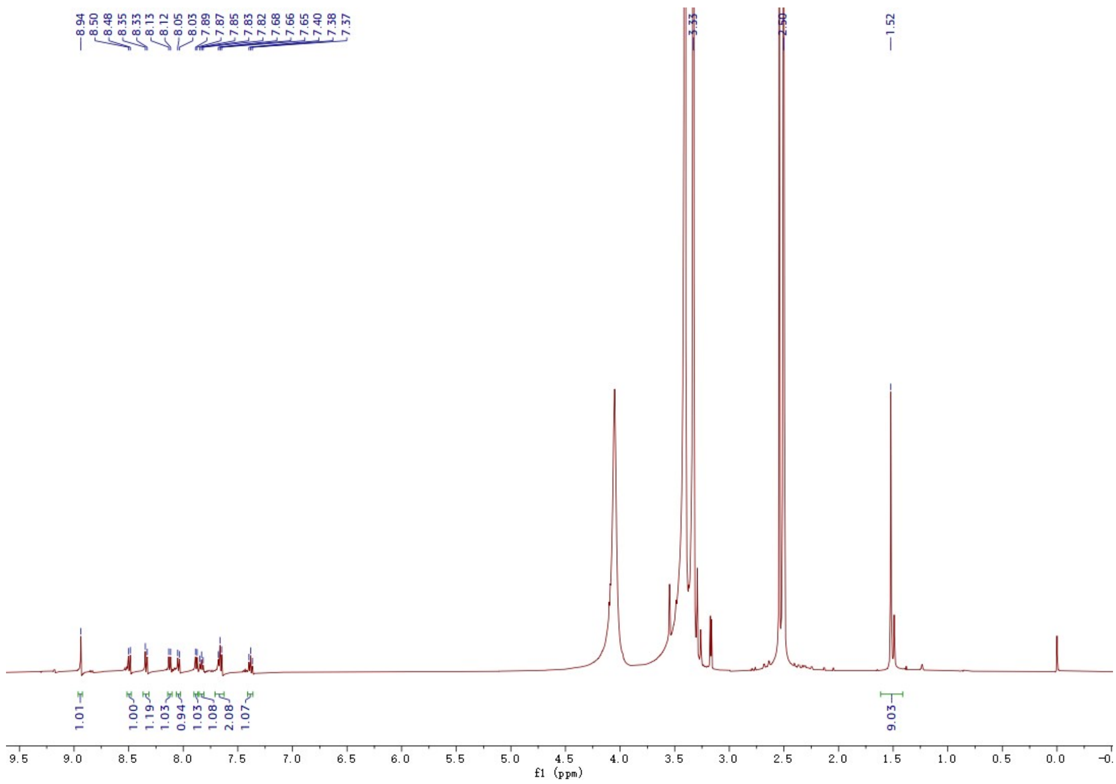

Figure S10. ^{1}H NMR (500MHz, DMSO-d_6) for **RhQ**.

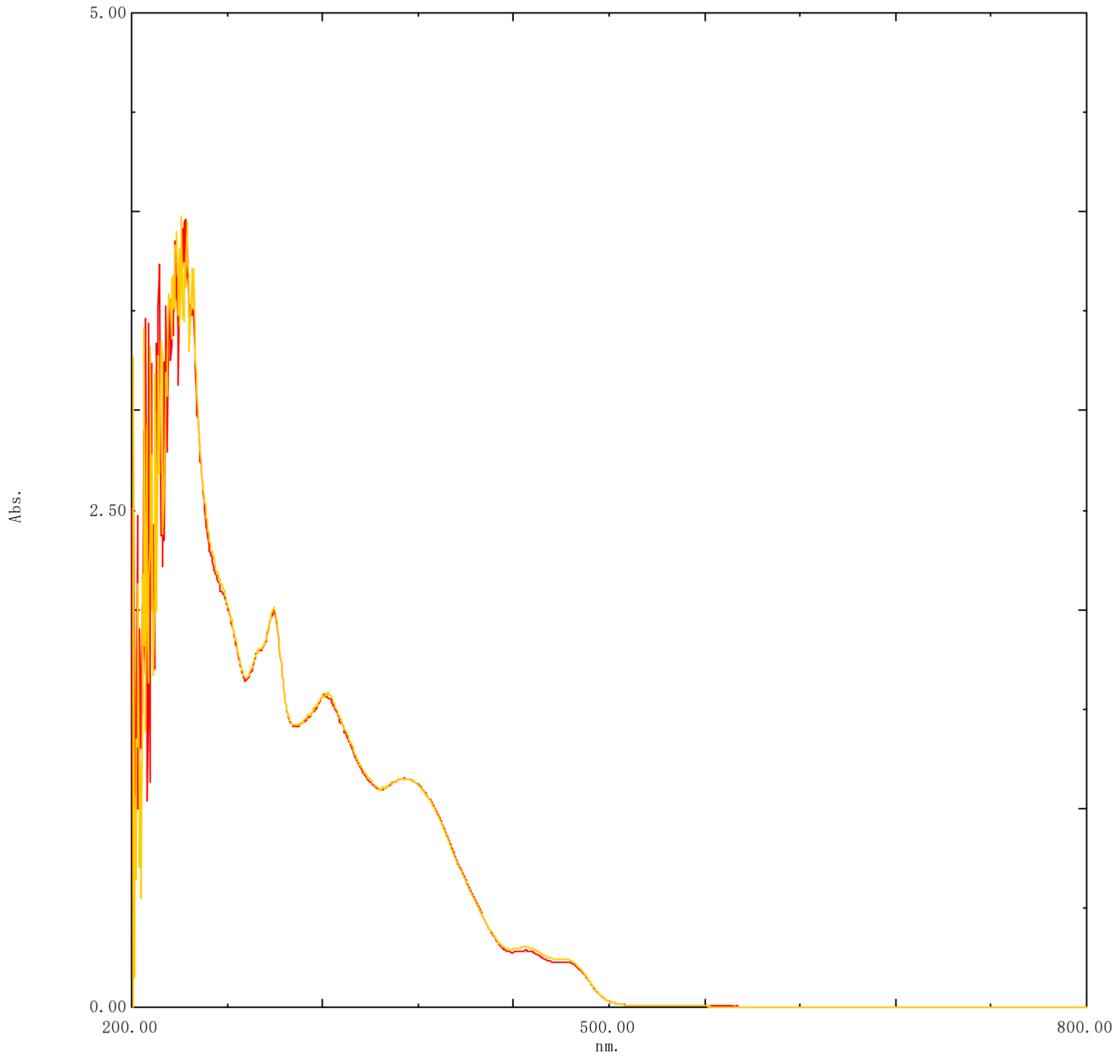

Figure S11. UV-Vis absorption spectra of **RhQ** (2.0×10^{-5} M) in Tris-HCl solution in the time course 0 h (yellow) and 24 h (red), respectively.

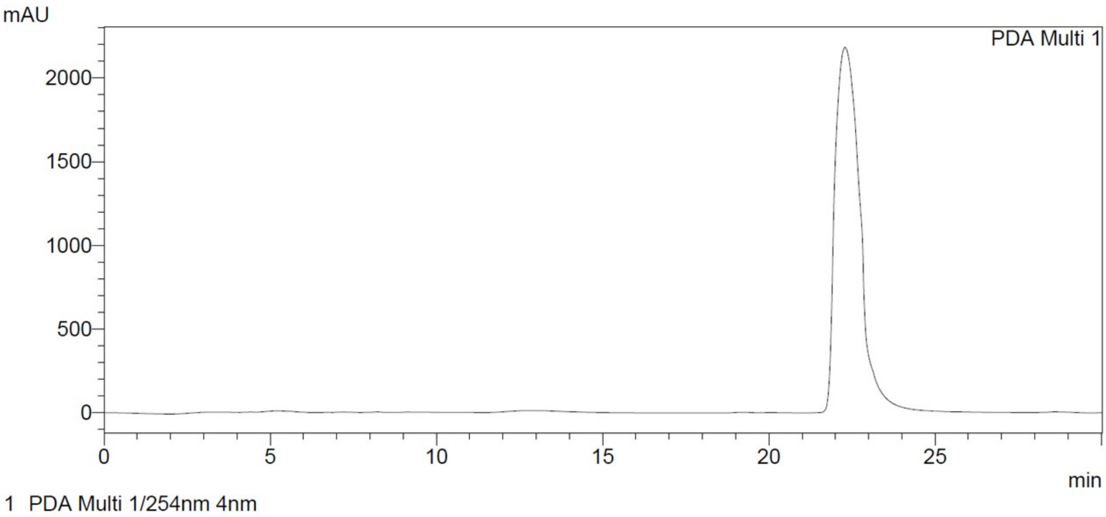

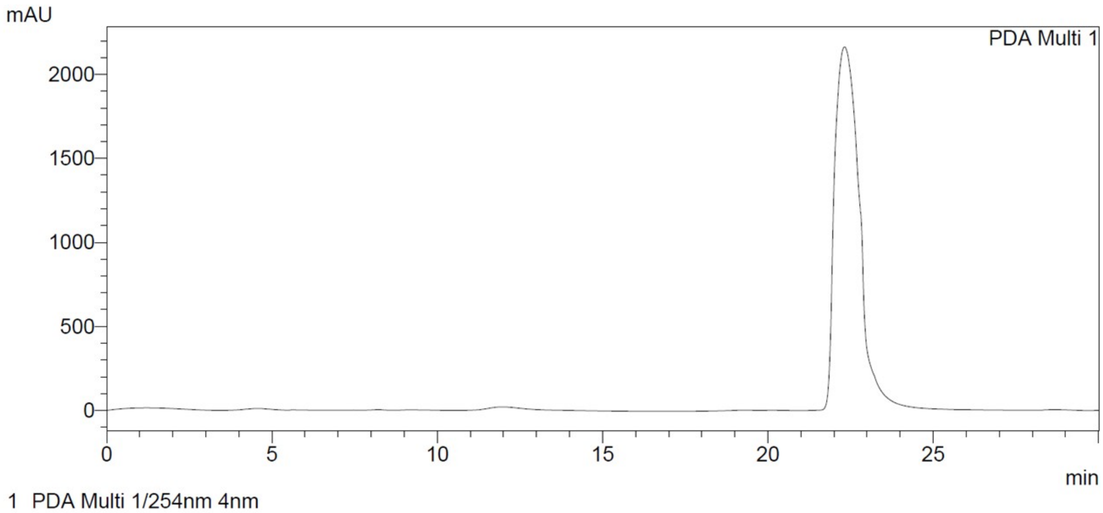

Figure S12. HPLC spectra for **RhS** (2.0×10^{-5} M) in TBS (Tris-HCl buffer solution, 10 mM, pH 7.35) solution with 0 h (up) and 24 h (down). Column: Inertsustain C18 column (LC-20AT, SPD-20A HPLC COLUMN, 150mm×5.0 μm I.D.). Column temperature: 40ºC. Mobile phase: methol/H_2O containing 0.01% TFA (90:10 methol/H_2O). Flow rate: 0.4 mL/min. Injection volume: 2.0×10^{-5} M.

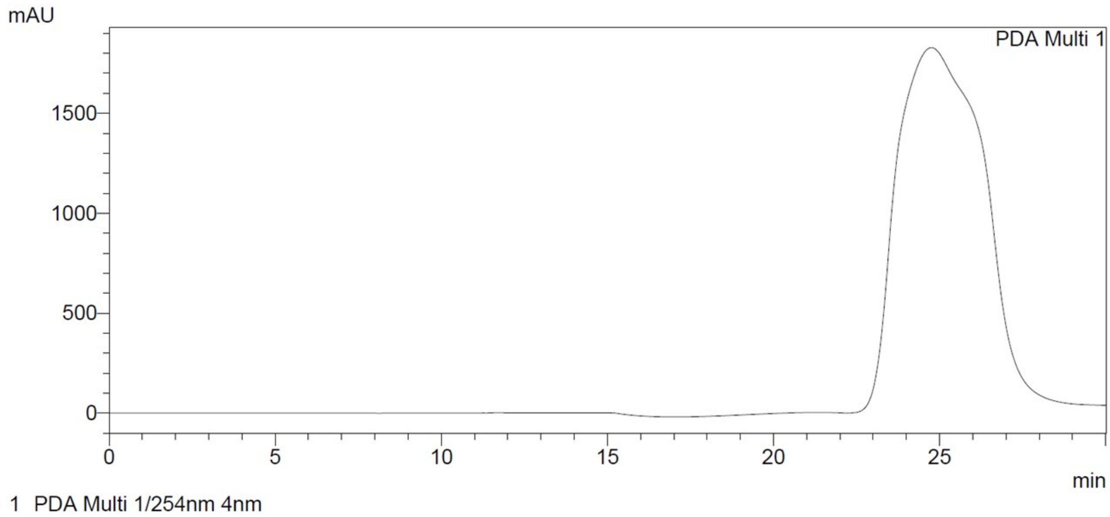

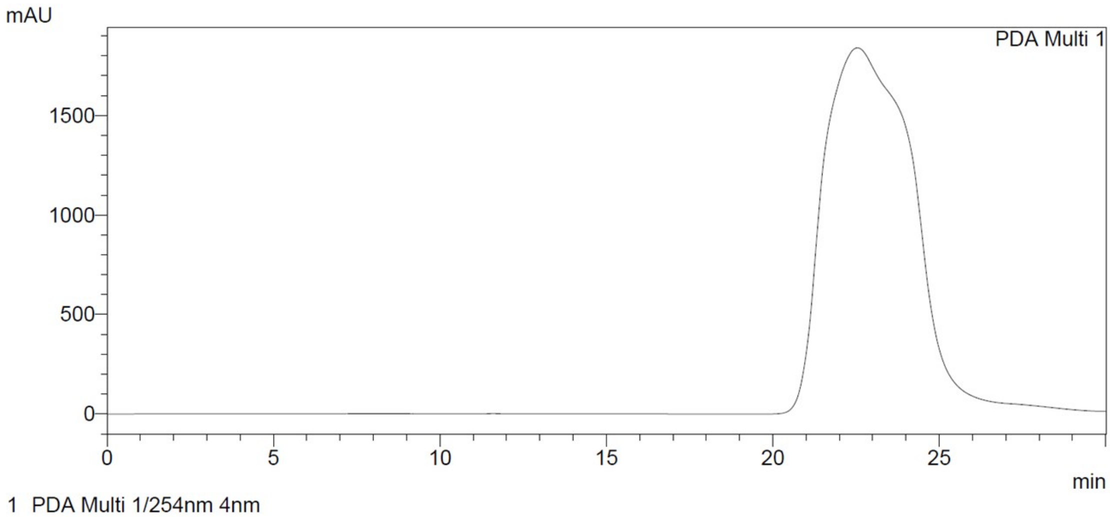

Figure S13. HPLC spectra for **RhQ** (2.0×10^{-5} M) in TBS (Tris-HCl buffer solution, 10 mM, pH 7.35) solution with 0 h (up) and 24 h (down). Column: Inertsustain C18 column (LC-20AT, SPD-20A HPLC COLUMN, 150mm×5.0 μm I.D.). Column temperature: 40ºC. Mobile phase: methol/H_2O containing 0.01% TFA (90:10 methol/H_2O). Flow rate: 0.4 mL/min. Injection volume: 2.0×10^{-5} M.

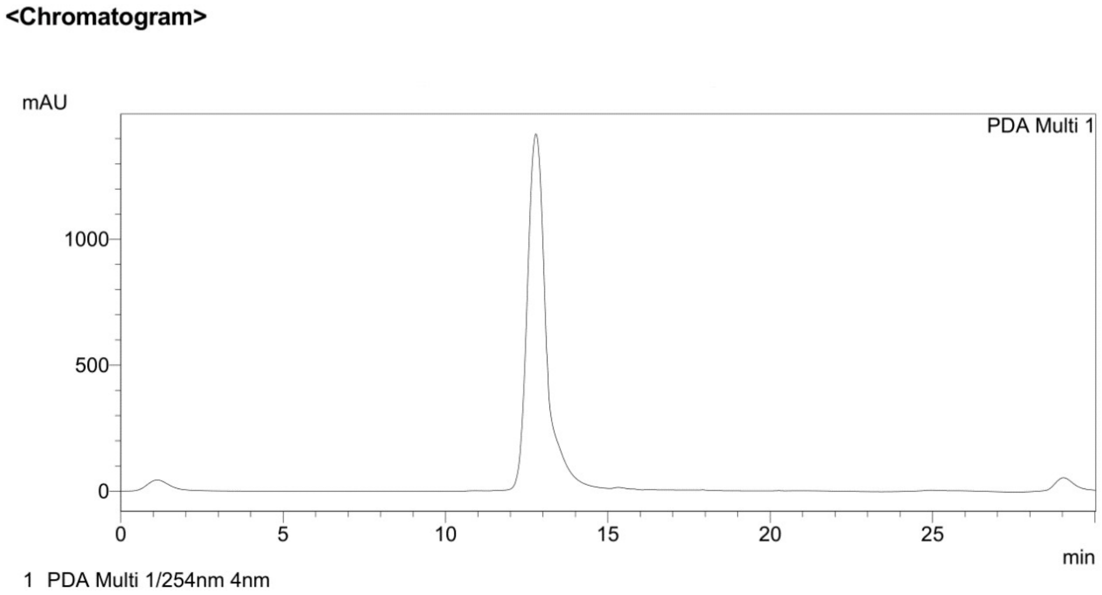

Figure S14. HPLC spectra for QB4 ligand (2.0×10^{-5} M) in TBS (Tris-HCl buffer solution, 10 mM, pH 7.35) solution with 0 h. Column: Inertsustain C18 column (LC-20AT, SPD-20A HPLC COLUMN, 150mm×5.0 μm I.D.). Column temperature: 40ºC. Mobile phase: methol/H_2O containing 0.01% TFA (90:10 methol/H_2O). Flow rate: 0.4 mL/min. Injection volume: 2.0×10^{-5} M.

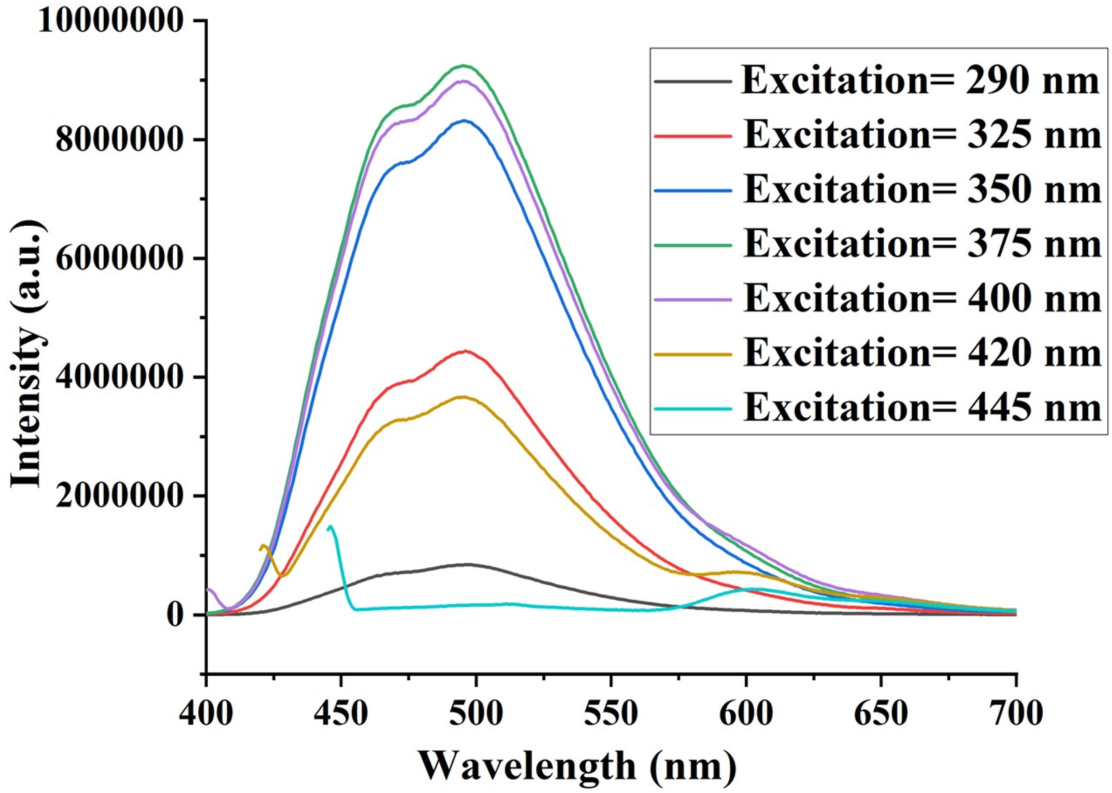

Figure S15. Fluorescence spectra of **RhQ** (2.0×10^{-5} M) recorded in Tris-HCl solution containing DMSO (1%v/v) followed by excitation at 290, 325, 350, 375, 400, 420 and 445 nm.

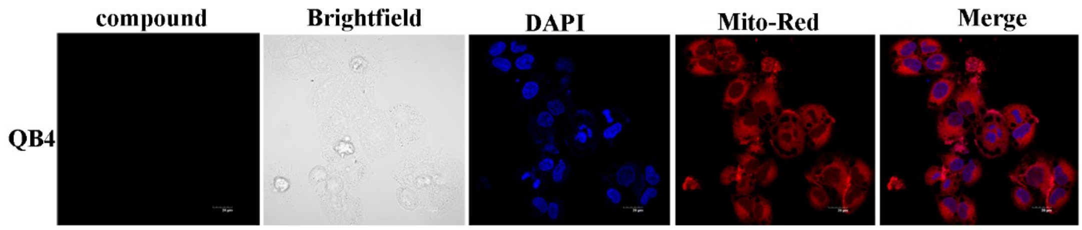

Figure S16. The colocalization of QB4 (39.8μM) in A549CDDP cells for 24 h with DAPI and Mito-Red by confocal microscopy. The λ_{ex}= 375 nm and λ_{em}= 500−540nm values of QB4.

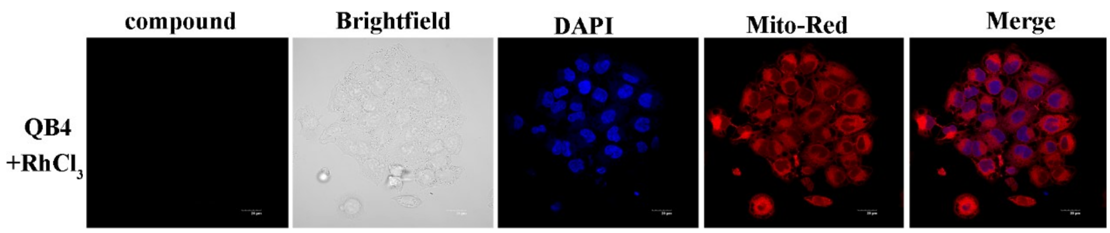

Figure S17. The colocalization of the mixed compounds (QB4 (0.08 μM)+

$RhCl_3 \cdot 3H_2O$ (0.08 μM)) in A549CDDP cells for 24 h with DAPI and Mito-Red by confocal microscopy. The λ_{ex} = 375 nm and λ_{em} = 500−540nm values of this mixed compounds.

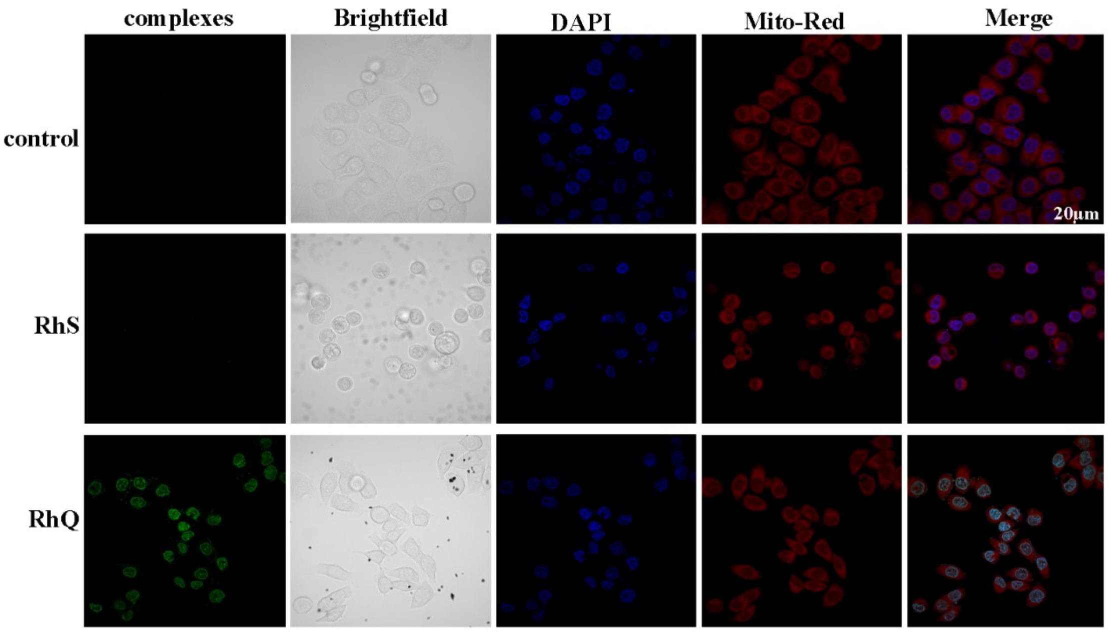

Figure S18. The colocalization of **RhS** (0.7 μM) and **RhQ** (0.08 μM) in A549CDDP cells for 24 h with DAPI and Mito-Red by confocal microscopy. The λ_{ex} = 375 nm and λ_{em} = 500−5400nm values of **RhS** and **RhQ**.

Table S13. RhS and **RhQ** induced DNA damage in A549CDDP cells.

Name	Head Area	Tail Area	Head DNA	Tail DNA	Head DNA%	Tail DNA%	Head Radius	Tail Length	Comet Length	Head MeanX	Tail MeanX	Tail Moment	Olive Tail Moment
control	2677	405	298.3	10.0	96.7	**3.3**	29	7	66	63.9	91.3	0.2	0.9
RhQ	1158	2840	194.9	173.2	52.9	**47.1**	19	99	138	51.2	93.5	46.6	19.9
RhS	892	1364	178.5	85.2	67.7	**32.3**	18	65	102	47.7	80.1	21.0	10.5

Table S14. The tumor volume in treated and non-treated mice from the date of surgery to the study end point in the A549CDDP xenograft model.

	mg/kg	1day (d)	3d			5d			7d		
		Tumor Volume (mm^3)	Tumor Volume (mm^3)	RTV	T/C%	Tumor Volume (mm^3)	RTV	T/C%	Tumor Volume (mm^3)	RTV	T/C%
Control	_	90.4±5.1	169.6±30.3	1.881±0.352	100.0	314.1±82.9	3.494±0.993	100.0	527.4±51.7	5.853±0.689	100.0
RhS	5.0	90.2±5.4	166.4±20.2	1.845±0.186	98.1	283.0±38.5	3.161±0.601	90.1	439.6±59.0*	4.891±0.742*	83.4
RhQ	5.0	90.9±6.1	158.0±10.4	1.745±0.181	93.2	267.9±17.5	2.951±0.182	84.5	384.6±12.5**	4.237±0.146**	72.9

	mg/kg	9d			11d			13d		
		Tumor Volume (mm^3)	RTV	T/C%	Tumor Volume (mm^3)	RTV	T/C%	Tumor Volume (mm^3)	RTV	T/C%
Control	_	765.1±54.9	8.462±0.448	100.0	973.7±71.3	10.768±0.481	100.0	1220. 1±135.0	13.502±1.437	100.0
RhS	5.0	586.6±83.9**	6.510±0.879**	76.7	669.9±57.8**	7.436±0.581**	68.8	741.5±37.9**	8.236±0.457**	60.8
RhQ	5.0	516.8±34.8**	5.697±0.440**	67.5	582.9±23.7**	6.430±0.435**	59.9	614.1±23.2**	6.773±0.424**	50.3

	mg/kg	15d		
		Tumor Volume (mm^3)	RTV	T/C%
Control	_	1427.8±155.9	15.789±2.223	100.0
RhS	5.0	765.8±43.0**	8.504±0.470**	53.6
RhQ	5.0	633.6±27.1**	6.989±0.480**	44.4

* p <0.05, ** p <0.01, p *vs* vehicle control (5.0% v/v DMSO/ saline vehicle).

Table S15. Average body weight in treated and non-treated mice from the date of surgery to the study end point in the A549CDDP xenogfart model.

	mg/kg	1 d	3 d	5 d	7 d	9 d	11 d	13 d	15 d
Control	_	19.8±0.5	19.9±0.5	20.1±0.5	20.2±0.5	20.4±0.5	20.5±0.5	20. 7±0.5	20.8±0.6
RhS	5.0	19.7±0.6	19.8±0.6	20.0±0.6	20.2±0.6	20.4±0.6	20.5±0.6	20.6±0.6	20.8±0.6
RhQ	5.0	19.7±0.5	19.8±0.5	20.0±0.5	20.1±0.5	20.3±0. 5	20.4±0.4	20.6±0.4	20.8±0.5

* p <0.05, ** p <0.01, p *vs* vehicle control (5.0% v/v DMSO/ saline vehicle).

Table S16. In Vivo Anticancer Activity of **RhS** and **RhQ** toward A549CDDP tumor xenograft.

	mg/kg	average tumor weight (mean ± SD, g)	inhibition of tumor growth (%)
Control	-	1.517±0.053	-
RhS	5.0	1.036±0.050**	46.4
RhQ	5.0	0.977±0.076**	55.3

* p <0.05, ** p <0.01, p *vs* vehicle control (5.0% v/v DMSO/ saline vehicle).

Original images for Figure 9:

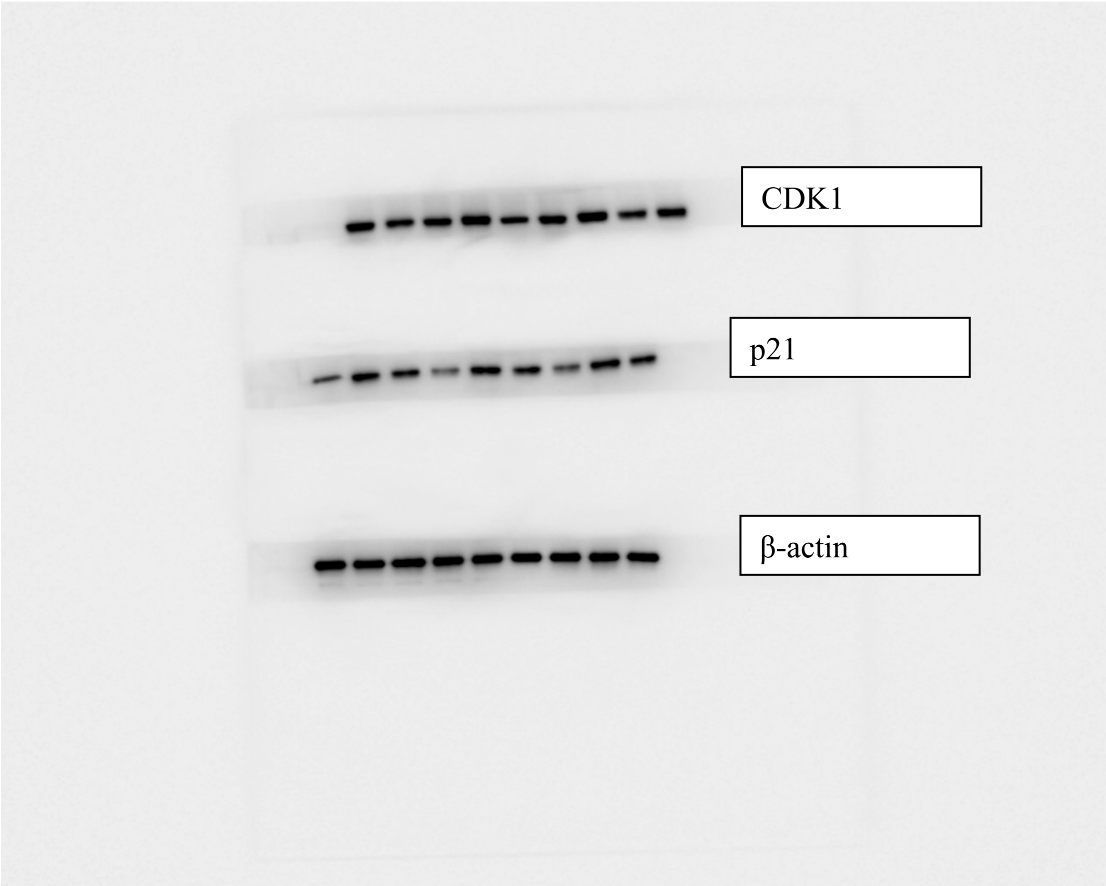

Methods

The other experimental methods

The antitumor mechanism of **RhN1**, **RhN2**, **RhS** and **RhQ** were performed as reported by Liu, Qin, Duan, Zhang and Galons[1-6].

1.1 Materials

The Tris, gel loading buffer, RNase A (100 μg/mL), 2-nitrobenzoic acid and propidium iodide (PI, 50 μg/mL) were purchased from Sigma. The antibody of cyclinB1, CDK1, p21, bax, cleaved caspase-3 and bcl-2 were purchased from Abcam. The tumor cell lines A549, A549CDDP and HL-7702 cells were obtained from the

Shanghai Institute for Biological Science (China). The Annexin V APC and 7-AAD double staining were purchased from FACS Aria II flow cytometer (BD Biosciences, San Jose, CA, USA).

1.2 Instruments

Elemental analyses (C, H, N) were carried out on a PerkinElmer series II CHNS/O 2400 elemental analyzer. NMR spectra were recorded on a Bruker AV-500 NMR spectrometer. Bioimaging assays were analyzed by confocal microscopy (Olympus FV3000). ESI-MS spectra were performed on Thermofisher Scientific Exactive LC−MS spectrometer (Thermal Elctronic, USA). The DNA damage were obtained on a fluorescent microscopy (Olympus BX43) at 25 °C. MTT assay were performed on M1000 microplate reader (Tecan Trading Co. Ltd., Shanghai, China). Cell cycle and apoptotosis analysis results were recorded on FACS Aria II flow cytometer (BD Biosciences, San Jose, CA, USA).

1.3 MTT assays

The each cell culture was maintained in RPMI-1640 medium supplemented with 10.0% fetal bovine serum (FBS), 100.0 U/mL penicillin, and 100.0 μg/mL streptomycin in 25.0 cm^2 culture flasks at 37 °C in a humidified atmosphere with 5.0% CO_2. All the cells to be tested in the following assays had a passage number of 3.0-6.0. The cells were seeded in 96 well plates at the density of 5000-8000 cells per well for 24 h, then incubated with different concentrations of **RhN1**, **RhN2**, **RhS** and **RhQ** for 24 h. Cell medium was discarded and MTT (1.0 mg/mL) was added. 4.0 h later, MTT solution was removed and DMSO was added. And obtained the results by a M1000 microplate reader (Tecan Trading Co. Ltd., Shanghai, China) at 570 nm.

1.4 Apoptotosis and bioimaging assay

Annexin V-FITC staining of the membranes was performed by using the Annexin V APC (which detects phosphatidylserine residues translocated from the inner to the outer cell membrane in early apoptotic stages) and 7-AAD (stains necrotic cells). The A549CDDP cells were incubated with **RhS** (0.7μM) and **RhQ** (0.08μM) for 24 h, and then stained with Annexin V APC (5 μL) and 7-AAD (5 μL) double staining, and analyzed by flow cytometry. Similar procedure was used for bioimaging assay (100 nM Mito-Red), and analyzed by confocal microscopy (Olympus FV3000).

1.5 Molecular docking experiments

The molecular docking simulations were performed with the aid of Autodock 4.2.6 software package (**G. M. Morris, R. Huey, W. Lindstrom, M. F. Sanner, R. K. Belew, D. S. Goodsell, A. J. Olson, J. Comput. Chem. 2009, 30, 2785-2791**) [5]. The crystal structure of DNA, with the PDB ID: 1BNA, was obtained from Protein Data Bank. The **RhS** and **RhQ** in this study were docked into both the major and minor binding sites of the DNA structure using Auto Dock tools (ADT). The information of the binding sites used in this study was the same as **Angew. Chem. Int. Ed. 2020, 59, 6420–6427** [5]. The nonpolar hydrogen atoms were merged and only the polar hydrogens remained. The Gasteiger charges were added to the DNA and **RhS** and **RhQ** molecules. A box size of 80 * 80 * 100 $Å^3$ with a grid spacing 0.375 Å was defined around the major or minor binding sites of the DNA. The grid map around the binding site of the DNA was generated by the probe atoms employing the Auto Grid program. Each grid in the map represents the potential energy of a probe atom in the presence of all the atoms of the DNA molecule. The docking simulation was performed with the Lamarckian Genetic Algorithm (LGA) with 1500000 iterations and was repeated 270000 times to generate 100 docking conformations of the compounds on the DNA molecule. Results were clustered with a rootmean- square distance (RMSD) of 2.0 Å. Clusters with the lowest binding energies were considered the most favorable conformations.

1.6 DNA damage assay

DNA damage assay was investigated by means of comet assay[2,3]. The A549CDDP cells in culture medium were incubated with different concentration of **RhS** (0.7μM) and **RhQ** (0.08μM) for 24 h at 37 °C. The A549CDDP cells were harvested by a trypsinization process at 24 h. A total of 100 mL of 0.5% normal agarose in PBS was dropped gently onto a fully frosted microslide, covered immediately with a coverslip, and then placed at 4 °C for 15 min. The coverslip was removed after the gel had been set. A mixture of 50 mL of the cell suspension (200 cells/mL) mixed with 50 mL of 1.0% low melting agarose was preserved at 37 °C. A total of 100 mL of this mixture was applied quickly on top of the gel, coated over the microslide, covered immediately with a coverslip, and then placed at 4 °C for 15 min. The coverslip was again removed after the gel had been set. A third coating of 50 mL of 0.5% low melting agarose was placed on the gel and allowed to place at 4 °C for 20 min. After solidification of the agarose, the coverslips were removed, and the slides were immersed in an ice-cold lysis solution (2.5 M NaCl, 100mM EDTA, 10mM Tris, 90mM sodium sarcosinate, NaOH, pH 10.0, 1.0% Triton X-100 and 10.0% DMSO) and placed in a refrigerator at 4 °C for 2.5 h. All of the above operations were performed under low lighting conditions to avoid additional DNA damage. The slides, after removal from the lysis solution, were placed horizontally in an electrophoresis chamber. The reservoirs were filled with an electrophoresis buffer (300mM NaOH, 1.2mM EDTA) until the slides were just immersed in it, and the DNA was allowed to unwind for 35 min in electrophoresis solution. Then the electrophoresis was carried out at 25 V and 300.0mA for 25 min. After electrophoresis, the slides were removed, washed thrice in a neutralization buffer (400mM Tris, HCl, pH 7.5). The A549CDDP cells were stained with 25 μL of EB (20.0 mg/mL) in the dark for 25min. The slides were washed in chilled distilled water for 15.0 min to neutralize the excess alkali, air-dried and scored for comets by fluorescent microscopy (Olympus BX43, magnification 200×).

1.7 Western Blot

The A549CDDP cells were incubated with **RhS** (0.7μM) and **RhQ** (0.08μM) for 24 h, and then the cells harvested from each well of the culture plates were lysed in 150.0 μL of extraction buffer consisting of 149.0 μL of RIPA lysis buffer and 1.0 μL of PMSF (100.0 mM). The suspension was centrifuged at 10 000 rpm at 4 °C for 10 min, and the supernatant (10μL for each sample) was loaded onto 10% polyacrylamide gel and then transferred to a microporous polyvinylidene difluoride (PVDF)membrane. Western blotting was performed using anti-apoptotic antibody, or anti-β-actin primary antibody and horseradish-peroxidase-conjugated anti-mouse or anti-rabbit secondary antibody. The protein bands were visualized using chemiluminescence substrate.

1.8 Anticancer activity toward A549CDDP in vivo

The A549CDDP cells were harvested and injected subcutaneously into the right flank of nude mice with 5×10^6 cells in 200 μL of serum-free medium. When the xenograft tumor growth to the volume about 1000 mm^3, the mice were killed and the tumor tissue were cut into about 1.5 mm^3 small pieces, and then transplanted into the right flank of female nude mice, When tumors reach a volume of 90-100 mm^3 on all mice, the mice were randomized into vehicle control and treatment groups (n=6/group), received the following treatments: (a) vehicle control, 5.0% v/v DMSO/ saline vehicle, (b) **RhS** at dose 5.0 mg/kg every two day (10% v/v DMSO/saline), (c) **RhQ** (5.0 mg/kg) via percutaneous injection every 2 days (q2d). The tumor volumes were determined every three days by measuring length (*l*) and width (*w*) and calculating volume, tumor volume and inhibition of tumor growth were calculated using formulas 1−3:

Tumor volume: $V = (w^2\times l)/2$ (1)

The tumor relative increment rate: $T/C\ (\%) = T_{RTV}/C_{RTV}\times100\%$ (2)

inhibition of tumor growth: $IR(\%) = (W_c - W_t)/W_c\times100\%$ (3)

Where w and l mean the shorter and the longer diameter of the tumor respectively; T_{RTV} and C_{RTV} was the RTV of treated group and control group respectively. (RTV: relative tumor volume, $RTV= V_t /V_0$); W_t and W_c mean the average tumor weight of complex-treated and vehicle controlled group respectively.

In addition, the A549CDDP xenograft mouse models were purchased from Changzhou Cavens Experimental Animal Co., Ltd (Jiangsu, China, Approval No. SCXK 2016-0010). The animal procedures were approved by Changzhou Cavens Experimental Animal Co., Ltd (Jiangsu, China, Approval No. SYXK (Su) 2017-0007). Further, all the experimental procedures were conducted in accordance with the NIH Guidelines for the Care and Use of Laboratory Animals. Animal experiments were approved by Changzhou Cavens Experimental Animal Co., Ltd ((Jiangsu, China).

1.9 Statistical analysis

The experiments of in vitro antiproliferative activity have been repeated from five times, and the results obtained are presented as means ± standard deviation (SD). Significant changes were assesses by using Student's t test for unpaired data, and p values of <0.01 were considered significant.

References

1 (a) Q.-P. Qin, Z.-Z. Wei, Z.-F. Wang, X.-L. Huang, M.-X. Tan, H.-H. Zou, H. Liang, Imaging and therapeutic applications of Zn(II)-cryptolepine–curcumin molecular probes in cell apoptosis detection and photodynamic therapy, *Chem. Commun.,* 2020, **56**, 3999–4002. (b) Z.-F. Chen, Q.-P. Qin, J.-L. Qin, Y.-C. Liu, K.-B. Huang, Y.-L. Li, T. Meng, G.-H. Zhang, Y. Peng, X.-J. Luo, H. Liang, Stabilization of G‑quadruplex DNA, inhibition of telomerase activity, and tumor cell apoptosis by organoplatinum(II) complexes with oxoisoaporphine, *J. Med. Chem.,* 2015, **58**, 2159−2179. (b) Z.-F. Wang, X.-F. Zhou, Q.-C. Wei, Q.-P. Qin, J.-X. Li, M.-X. Tan, S.-H. Zhang, Novel bifluorescent Zn(II)–cryptolepine–cyclen complexes trigger apoptosis induced by nuclear and mitochondrial DNA damage in cisplatin-resistant lung tumor cells, *Eur. J. Med. Chem.*, 2022, **238**, 114418. (c) Z.-F. Wang, Q.-X. Nong, H.-L. Yu, Q.-P. Qin, F.-H. Pan, M.-X. Tan, H. Liang, S.-H. Zhang, Complexes of Zn(II) with a mixed tryptanthrin derivative and curcumin chelating ligands as new promising anticancer agents, *Dalton Trans.*, 2022, **51**, 5024–5033.

2 B. Tang, D. Wan, Y.-J. Wang, Q.-Y. Yi, B.-H. Guo, Y.-J. Liu, An iridium(III) complex as potent anticancer agent induces apoptosis and autophagy in B16 cells through inhibition of the AKT/Mtor pathway, *Eur. J. Med. Chem.,* 2018, **145**, 302–314.

3 C.-C. Zeng, S.-H. Lai, J.-H. Yao, C. Zhang, H. Yin, W. Li, B.-J. Han, Y.-J. Liu, The induction of apoptosis in HepG-2 cells by ruthenium(II) complexes through an

intrinsic ROS-mediated mitochondrial dysfunction pathway, *Eur. J. Med. Chem.,* 2016, **122**, 118–126.

4 M. Li, C. Du, N. Guo, Y. Teng, X. Meng, H. Sun, S. Li, P. Yu, H. Galons, Composition design and medical application of liposomes, *Eur. J. Med. Chem.,* 2019, **164**, 640–653.

5 (a) X. Li, J. Wu, L. Wang, C. He, L. Chen, Y. Jiao, C. Duan, Mitochondrial-DNA-targeted Ir^{III}-containing metallohelices with tunable photodynamic therapy efficacy in cancer cells, *Angew. Chem. Int. Ed.,* 2020, **59**, 6420–6427. (b) G. M. Morris, R. Huey, W. Lindstrom, M. F. Sanner, R. K. Belew, D. S. Goodsell, A. J. Olson, AutoDock4 and autoDockTools4: automated docking with selective receptor flexibility, *J. Comput. Chem.,* 2009, **30**, 2785–2791.

6 (a) M. Li, C. Du, N. Guo, Y. Teng, X. Meng, H. Sun, S. Li, P. Yu, H. Galons, Composition design and medical application of liposomes, *Eur. J. Med. Chem.,* 2019, **164**, 640–653. (b) Y. Ai, B. Zhu, C. Ren, F. Kang, J. Li, Z. Huang, Y. Lai, S. Peng, K. Ding, J. Tian, Y. Zhang, Discovery of new monocarbonyl ligustrazine-curcumin hybrids for intervention of drug-sensitive and drug-resistant lung cancer, *J. Med. Chem.,* 2016, **59**, 1747–1760.